

Integrated Bus Conductors Improve System Performance In Modular Drives

David A. Torrey* James M. Kokernak† Erkan Mese† Yilmaz Sozer†

*Department of Electric Power Engineering
Rensselaer Polytechnic Institute
Troy, NY 12180-3590, USA

†Advanced Energy Conversion, LLC
31 Ontario Street
Cohoes, NY 12047, USA

Abstract

This paper examines the application of printed circuit boards (PCBs) as an integral part of a power electronic converter. Used in this way, the PCB offers the opportunity to reduce prototype and manufactured costs, as well as reduce prototype lead time. The issues surrounding such an application are largely thermal. The paper shows how to construct a simple analytic thermal model of the PCB to aid in design. This model is compared with experimental results for a PCB used to support the inverter circuit within a switched-reluctance generator system.

1 Introduction

This paper discusses using printed circuit boards (PCBs) as an integral part of electronic power converters. We have found this technique extremely useful in creating a compact, easy to manufacture structure that has beneficial electromagnetic behavior. We have successfully applied this technique to converters processing up to 20 kW using 0.070 mm thick copper cladding. Thicker copper can support much higher power levels.

The approach described here competes to some extent with laminated bus bars [1]. While laminated bus bars offer greater packaging flexibility than a printed circuit board, the PCB can offer a much less expensive approach. The PCB is generally restricted to planar structures. While this can often be accommodated in many power converters, it cannot be accommodated in all power converters. Further, the ability to custom-shape laminated bus bars allows integrating them into the overall converter package,

perhaps reducing the number of interconnects in the process. The optimal partitioning between laminated bus bars and PCBs depends on the specific system objectives.

The fundamental issues with using PCBs to support a power converter are thermal in nature. Heat generated within the conductors of the laminated structure must be driven off into the surroundings, suggesting that heat transfer through both conduction and convection figure prominently in determining acceptable current limits. While heat transfer is fundamentally a three-dimensional field problem with time dependence, the planar structure being analyzed lends itself to one-dimensional steady state analysis. Of principal concern to us is determination of PCB performance in the face of the potentially large currents flowing in the power converter. The currents found within a power converter can easily exceed those considered in the design of PCB traces [5, 7]. Further, our approach is generally based on using large copper zones where it is a much more complicated issue to determine where currents are flowing at any particular time.

The printed circuit structure considered in this paper is shown in Fig. 1. This is a four layer PCB, with the layers of copper conductor separated by a fiberglass-filled epoxy. The standard copper cladding is usually specified by weight of copper per square foot of area. Table 1 gives typical cladding thicknesses. The fiberglass-filled epoxy used in standard printed circuit boards adheres to a NEMA standard; grade FR-4 is considered in this paper [4]. Pertinent thermophysical properties of copper and FR-4 are given in Table 2; these properties have been collected from the sources cited. Standards related to printed circuit boards include [4, 5] among others; Shugg provides a detailed list of pertinent standards

from NEMA, IPC and ANSI [6].

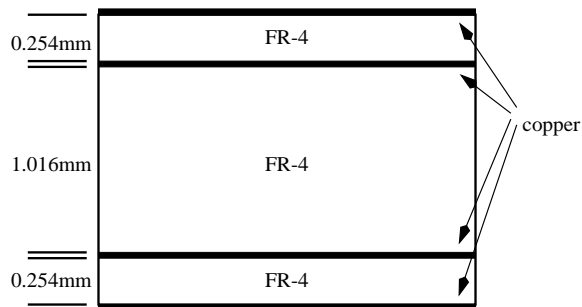


Figure 1: The cross-section of a typical four layer PCB.

Table 1: Typical cladding thicknesses for PCBs [7].

Cladding Designation	Thickness (mm)	Thickness (in)
1 oz	0.035	0.0014
2 oz	0.070	0.0028
3 oz	0.105	0.0041
4 oz	0.140	0.0055
10 oz	0.35	0.0138

After a short primer on conduction heat transfer and convection heat transfer, we turn our attention to the thermal analysis of a four-layer printed circuit board structure. Our objective is to estimate the current densities that can be supported by these structures when used in power converters. Following this, we experimentally examine the performance of a PCB used to support the dc bus of a 6kW switched-reluctance starter/alternator; the performance of this system is documented in [9, 10]. The paper concludes with a discussion of manufacturing issues that need to be considered as the concept is taken to higher power levels.

2 Heat Transfer Considerations

This section discusses the basics of conduction and convection heat transfer. This material is put to use in Sec. 3 to develop a thermal model of the four-layer PCB of Fig. 1. A more complete discussion of these

issues can be found in any good heat transfer text, [2, 3] are two examples.

2.1 Conduction Heat Transfer

Conduction heat transfer is the only mode of heat transfer within opaque solids, and is facilitated by the tight thermal coupling of the molecules that form the solid. Conduction is the mechanism by which the thermal energy of each molecule is shared with its adjacent neighbors. The temperature distribution within a thermally conducting solid is dictated by Fourier's Law of heat conduction and conservation of energy. Generally, the temperature distribution is a function of both space and time.

Conservation of thermal energy within a conducting solid accounts for thermal energy flowing in, thermal energy flowing out, heat being generated within the solid and the storage of thermal energy. In Cartesian coordinates, energy conservation can be expressed as

$$-\frac{\partial \hat{q}_x}{\partial x} - \frac{\partial \hat{q}_y}{\partial y} - \frac{\partial \hat{q}_z}{\partial z} + \dot{q} = \rho c \frac{\partial T}{\partial t} \quad , \quad (1)$$

where \hat{q}_x , \hat{q}_y , \hat{q}_z are the x-, y-, and z-directed heat fluxes, respectively, \dot{q} is the heat generated per unit volume, ρ is the density, c is the heat capacity, T is the temperature, and t is time. It should be noted that the heat flux is heat per unit area and is a vector quantity. Equation 1 can be written more succinctly as

$$-\nabla \cdot \vec{\hat{q}} + \dot{q} = \rho c \frac{\partial T}{\partial t} \quad . \quad (2)$$

The use of the divergence operator generalizes the expression to any right-hand coordinate system.

Fourier's law of heat conduction is

$$\vec{\hat{q}} = -k \vec{\nabla} T \quad , \quad (3)$$

where k is the thermal conductivity. Equation 3 allows us to put Eq. 2 entirely in terms of temperature and thermophysical constants:

$$\nabla^2 T + \frac{\dot{q}}{k} = \frac{1}{\alpha} \frac{\partial T}{\partial t} \quad , \quad (4)$$

where $\alpha = k/(\rho c)$ is called the thermal diffusivity and describes how quickly heat diffuses through the material. Equation 4 assumes that k is not a function of location within the solid. In Eq. 4, temperature is the dependent variable. This equation is in the general form of a diffusion equation and describes how temperature evolves spatially and temporally. That is, $T = T(x, y, z, t)$ in a Cartesian coordinate system. Because T varies as a function of

Table 2: Thermophysical properties for a PCB based on FR-4 [3, 4, 7, 6].

Property	Copper	FR-4	SI Units
Density	8950	1800	kg/m ³
Thermal Conductivity	385	0.293	W/m · C
Heat Capacity	386	1570	J/kg · C
Thermal Diffusivity	1.114×10^{-4}	1.037×10^{-7}	m ² /s
Thermal Expansion Coef.	17×10^{-6}	9×10^{-6}	K ⁻¹

position and time, we can refer to T as a scalar field. Similarly, we can refer to \hat{q} as a vector field. While Eq. 4 is very cumbersome analytically for all but the simplest of cases, it can be solved numerically through finite element analysis or other numerical techniques.

For the important case of steady conduction in one direction without internal heat generation, Eq. 4 can be integrated twice to reveal that the temperature distribution is linear in the direction of heat flow. This allows us to establish an analogy between the flow of heat and the flow of electricity through a resistor. Table 3 summarizes the analogy between electrical and thermal conduction. The thermal resistance offered by a solid is given by

$$R_{th} = \frac{l}{kA} \quad , \quad (5)$$

where l is the length of the conductor in the direction of heat flow, k is the thermal conductivity, and A is the cross-sectional area normal to the heat flow. The analogy can be extended to include heat generation; this additional term serves as a heat source, the thermal analog of a current source.

Unsteady heat conduction implies that the temperature distribution is changing with time. This requires simultaneous consideration of spatial and temporal terms, a much more intimidating situation than the case of steady conduction. In one dimension, this problem can be handled analytically by breaking our thermal conductor into smaller pieces, with each piece represented by a resistor and a capacitor. The resistance is given by Eq. 5; the capacitance is given by

$$C_{th} = \rho l A c \quad , \quad (6)$$

where ρ is the density, l is the length in the direction of heat flow, A is the area normal to the heat flow, and c is the heat capacity of the material. Since the thermal capacitance is placed in parallel with the

thermal resistance, the thermal capacitance always acts to reduce the thermal impedance. This explains the shape of the transient thermal impedance curves for power semiconductors.

There are generally two situations in which it is justified to ignore the thermal capacitance. The first is when the thermal resistance is small compared with other thermal resistances in the system. This allows one to treat the conductors with small resistances as bodies with uniform temperature. The second situation is when the worst-case temperature distribution is desired. Since the thermal capacitance always acts to reduce the overall resistance, ignoring the capacitance will project maximum temperature rise. For both of these reasons, we will not consider the effect of thermal capacitance in our model of a PCB.

2.2 Convection Heat Transfer

Convective heat transfer involves a moving fluid, implying a coupling between the fluid mechanics which describe the motion of the fluid and the heat transfer which is taking place. This coupling makes the heat transfer process extremely difficult to describe analytically. This section motivates the use of empirical correlations for the description of convective heat transfer. We use these correlations to describe the heat transfer coefficient that figures prominently in Newton's law of cooling:

$$\hat{q} = \bar{h} (T_w - T_\infty) \quad , \quad (7)$$

where \hat{q} is the heat flux normal to the solid surface, \bar{h} is the mean heat transfer coefficient, T_w is the temperature of the solid surface and T_∞ is the temperature of the fluid away from the solid surface. As we will see below, the heat transfer coefficient is nonlinear because it depends on fluid properties that are nonlinear functions of temperature.

Most convection heat transfer problems involve the use of empirical correlations that describe the heat

Table 3: A summary of the electrical and thermal analogy.

Electrical		Thermal	
Quantity	Symbol	Symbol	Quantity
Current	i	q	Heat
Potential Difference	$v_1 - v_2$	$T_1 - T_2$	Temperature Difference
Resistance	R_e	R	Resistance
Conductivity	σ	k	Conductivity
Current Density	J	\hat{q}	Heat Flux

transfer coefficient. In order to make the correlations apply to as many different problems as possible, most correlations are tied to dimensionless groups, or numbers, which describe the major fluid mechanical behavior associated with the problem. This section takes a rather pragmatic approach to describing the use of convection correlations.

2.2.1 Dimensionless Groups

To begin, we identify the dimensionless groups that describe free convection. Forced convection would use different dimensionless groups, but the idea is still to characterize the thermo-fluid mechanics in as generic a way as possible. Here we focus on free convection because this is not only the worst case for heat transfer, but it is probably also the most applicable.

Convection heat transfer occurs through a boundary region local to the solid. The description of the temperature profile in the boundary region is generally dependent on the momentum (velocity) profile in the boundary region. The coupling between the temperature and momentum is expressed through the Prandtl number:

$$\text{Pr} = \frac{c_p \mu}{k} = \frac{\nu}{\alpha} \quad , \quad (8)$$

where c_p is the heat capacity for constant pressure, μ is the dynamic viscosity, k is the thermal conductivity (of the fluid), ν is the kinematic viscosity and α is the thermal diffusivity. The Prandtl number is the (dimensionless) ratio of momentum and thermal diffusivities and ties the evolution of the thermal boundary layer to that of the momentum boundary layer.

In free convection the fluid motion is driven by the change in fluid density as a function of temperature. As a fluid warms, its density decreases making

it more buoyant. The competition between buoyancy forces and inertial forces dictates how much fluid motion results. The competition between the buoyancy and inertial forces is summarized by the Grashof number:

$$\text{Gr}_x = \frac{\beta \Delta T g x^3}{\nu^2} \quad , \quad (9)$$

where β is the volume expansivity, $\Delta T = T_w - T_\infty$, and g is the gravitational constant. The subscript on the Grashof number indicates the characteristic length associated with the calculation; the characteristic length is dependent on the specific correlation. It is worth noting that the volume expansivity for an ideal gas is the reciprocal of its absolute temperature. Some free convection correlations are tied to the product of the Prandtl number and the Grashof number. This is called the Rayleigh number:

$$\text{Ra}_x = \text{Gr}_x \text{Pr} = \frac{\beta \Delta T g x^3}{\alpha \nu} \quad . \quad (10)$$

The final dimensionless number is the heat transfer coefficient. This is the Nusselt number:

$$\overline{\text{Nu}}_x = \frac{\bar{h} x}{k} \quad , \quad (11)$$

where \bar{h} is the average heat transfer coefficient used in Newton's law of cooling, Eq. 7. The Nusselt number is tied to the Prandtl, Grashof and Rayleigh numbers through an empirical correlation that represents the fit of an equation to experimental data. The fluid properties for all of these dimensionless numbers are evaluated at the film temperature, T_f , defined as

$$T_f = \frac{T_w + T_\infty}{2} \quad . \quad (12)$$

2.2.2 Empirical Correlations

For free convection, we generally have

$$\overline{\text{Nu}}_x = f(\text{Ra}_x) \quad , \quad (13)$$

where the functional form is based on fitting an equation to experimental data. The functional form depends heavily on the orientation of the rigid body that is driving heat into the fluid that surrounds it. Generally, the more vertical the orientation the more favorable heat transfer while a more horizontal orientation is less favorable to heat transfer. The overbar applied to the Nusselt number indicates that this is a mean quantity representative of the entire plate; locally the Nusselt number can vary by location on the surface.

Here, we assume the PCB to be in a horizontal orientation. Other situations can be handled similarly. Mills [3] gives two correlations for heated horizontal plates facing down. For a square plate with side length L ,

$$\overline{\text{Nu}}_L = 0.82 \text{Ra}_L^{1/5} \quad ; \quad 10^5 < \text{Ra}_L < 10^{10} \quad . \quad (14)$$

A more general correlation for a rectangular plate with shorter side L and longer side W is

$$\begin{aligned} \overline{\text{Nu}}_L = & 6.5 \left[1 + 0.38 \frac{L}{W} \right] \times \\ & \left[(1 + 13.5 \text{Ra}_L^{-0.16})^{0.39} - \right. \\ & \left. (13.5 \text{Ra}_L^{-0.16})^{0.39} \right] \text{Ra}_L^{0.13} \quad , \quad (15) \end{aligned}$$

where

$$10^6 < \text{Ra}_L < 10^{10} ; 0.7 < \text{Pr} < 4800 \quad .$$

For a horizontal heated plate facing up, the appropriate correlation is

$$\overline{\text{Nu}}_L = 0.54 \text{Ra}_L^{1/4} \quad , \quad (16)$$

for

$$10^5 < \text{Ra}_L < 2 \times 10^7 \quad ;$$

and

$$\overline{\text{Nu}}_L = 0.14 \text{Ra}_L^{1/3} \quad , \quad (17)$$

for

$$2 \times 10^7 < \text{Ra}_L < 3 \times 10^{10} \quad .$$

It is worthy of note that the mean Nusselt number is always larger on the top surface than the bottom surface for a heated plate, suggesting that a worst-case calculation would be based on either Eq. 14 or Eq. 15.

2.2.3 Analysis Procedure

Based on the two previous subsections, we can now outline a procedure to determine the heat transfer coefficient \overline{h} associated with a solid/fluid interface:

1. Compute the film temperature T_f using Eq. 12.
2. Extract and calculate, as appropriate, fluid parameters k , c_p , μ , ν , ρ , α , and β from tables.
3. Calculate the Rayleigh number according to Eq. 10.
4. Select the appropriate correlation based on orientation and circumstances.
5. Calculate the mean Nusselt number using the correlation.
6. Calculate the heat transfer coefficient \overline{h} from Eq. 11.

2.3 Integrated Modeling of Conduction and Convection

Inevitably, every thermal conduction problem merges into a convection problem. It is very useful to approach the two problems from a unified perspective. As we have already discussed, conduction can be modeled with an electric circuit consistent with Table 3. Based on the form of Eq. 7, we can observe that Newton's law of cooling fits very naturally into our electric circuit analogy where

$$R_{\text{convection}} = \frac{1}{\overline{h}A} \quad , \quad (18)$$

where A is the area over which the fluid and solid are in contact. This resistive model of the convection interface forms the basis for the thermal resistance cited in heat sink literature.

3 Thermal Model of a PCB

This section develops a model of the PCB shown in Fig. 1. To do this, we use the information provided in the previous section to formulate the thermal resistances for conduction and convection heat transfer.

3.1 Assumptions

Certain assumptions are in order as we develop the model. These assumptions are driven either by the need to make the problem analytically tractable, or by the physical application of the PCB as its performance is evaluated in Sec. 4. We make the following assumptions when analyzing the PCB of Fig. 1:

1. The PCB is made with 0.070mm (2 ounce) cladding.
2. The PCB is square, measuring 318mm on a side.
3. The PCB is oriented horizontally.
4. The predominant direction of heat flow is in the vertical direction.
5. The four layers of conductor are symmetric. That is, there is as much current flowing through the upper two layers as there is flowing through the lower two layers. This suggests that there is no heat transfer between the two inner layers.
6. Due to the assumed symmetry, only the lower half of the board needs to be modeled. The lower half is chosen because heat flow is more restricted through the bottom of the board than through the top.
7. The air surrounding the PCB is free to move only due to convection currents.
8. The temperatures of the copper layers are sufficiently close to use the same thermal conductivity for each.
9. The solder mask is taken to be so thin that its thermal resistance is negligible.
10. Heat loss by radiation is negligible.

3.2 The Model

An electric circuit analog for the thermal model of the PCB is shown in Fig. 2. The current sources are used to represent the heat generated within the copper conductors on layers three (P_{I3}) and four (P_{I4}). There is one resistor for each layer of copper (R_{Cu}) and one resistor for the FR-4 (R_{FR-4}) core between the two copper layers. There is a resistance (R_{conv}) used to represent the convection interface between

Table 4: The properties of air for a film temperature of 17 °C [3].

β	0.00345	K ⁻¹
k	0.0261	W/m · K
ρ	1.220	kg/m ³
c_p	1007	J/kg · K
μ	18.02×10^{-6}	kg/m · s
ν	14.77×10^{-6}	m ² /s
Pr	0.69	
α	21.2×10^{-6}	m ² /s

the bottom layer of copper and the surrounding air. The datum for the model of Fig. 2 is the ambient temperature T_∞ .

Property values for air at a film temperature of 17 °C (290 K) are given in Table 2. This is close to the value encountered during the experimental investigation discussed in Sec. 4.

Calculations for the resistances in Fig. 2, subject to the stated assumptions are:

$$R_{Cu} = \frac{0.00007}{385 \times 0.318^2} = 1.789 \times 10^{-6} \text{ } ^\circ\text{C/W} \quad ; \quad (19)$$

$$\begin{aligned} R_{FR-4} &= \frac{0.000254}{0.293 \times 0.318^2} \\ &= 8.53 \times 10^{-3} \text{ } ^\circ\text{C/W} \quad ; \quad (20) \end{aligned}$$

$$\begin{aligned} Ra_L &= \frac{0.00345 \times 3 \times 9.81 \times 0.318^3}{(2.12 \times 10^{-5}) \times (14.77 \times 10^{-6})} \\ &= 1.043 \times 10^7 \quad ; \quad (21) \end{aligned}$$

$$\overline{Nu}_L = 0.82 (1.043 \times 10^7)^{1/5} = 20.771 \quad ; \quad (22)$$

$$\bar{h} = \frac{20.771 \times 0.0261}{0.318} = 1.705 \quad ; \quad (23)$$

$$R_{conv} = \frac{1}{1.705 \times 0.318^2} = 5.8 \text{ } ^\circ\text{C/W} \quad ; \quad (24)$$

To estimate the power dissipation within the PCB, we must estimate the resistance offered by the PCB traces (or copper zones) and the current flowing through this resistance. For the PCB application considered here, we note that there are six IGBT modules that are symmetrically arranged under the PCB. The mean length of conductor between the modules and the dc bus connection points is taken

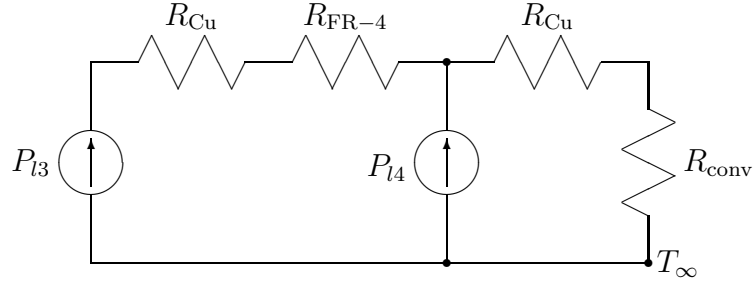


Figure 2: A thermal model for the lower half of the PCB shown in Fig. 1.

as 250 mm. The mean width of the current path is taken as 25 mm, the width of the conductor at the IGBT terminal. There are four of these conductor paths on the board within each layer. These conduction paths support the one-half of the rms phase currents as the phase currents combine to form the dc bus current. The factor of one-half assumes that the current divides equally between the two layers supporting each side of the dc bus.

To begin, the electrical conductivity of copper is taken to be

$$\sigma_{\text{Cu}} = \frac{5.903 \times 10^7}{1 + (4.3 \times 10^{-3})(T - 20^\circ\text{C})} \quad . \quad (25)$$

This makes the resistance of each path

$$R_e = \frac{0.25}{(5.98 \times 10^7) \times 0.025 \times 0.00007} = 2.4 \text{ m}\Omega \quad . \quad (26)$$

With each phase conducting 15 A of current, the estimated dissipation within each layer of the PCB is

$$P_{l3} = P_{l4} = 4 \times (2.4 \times 10^{-3}) \times 7.5^2 = 0.54 \text{ W} \quad . \quad (27)$$

With this level of dissipation, analysis of the circuit in Fig. 2 gives the expected steady-state temperature rise of the PCB surface to be

$$T_{\text{rise}} = (P_{l3} + P_{l4}) R_{\text{conv}} = 6.26 \text{ }^\circ\text{C} \quad . \quad (28)$$

4 Experimental Results

This section experimentally examines the performance of the PCB structure of Fig. 1 in support of a switched-reluctance generator (SRG) system generating 5.7 kW into a 300 V dc bus. Other performance measures for this system have been documented in

the literature [9, 10]. The PCB implemented in this system is comprised of four layers, two each for the positive and negative sides of the dc bus. The PCB mounts directly to the IGBT modules used to form the power circuit. Connections to the SRG are made directly from the IGBT modules. The positive and negative dc bus are interleaved to give symmetry and to maximize the parasitic capacitance associated with the structure. The dimensions of the PCB are consistent with the assumptions and calculations of Sec. 3.

The temperature distribution for the PCB and its surroundings is monitored with ten thermocouples. Six of the thermocouples are glued to the bottom of the PCB. One of the thermocouples is glued to the top of the PCB. One thermocouple is glued to the inside top of the inverter enclosure. One thermocouple monitors the inlet coolant temperature and one thermocouple monitors the outlet coolant temperature. Each of the ten thermocouples are sampled every 5 s, with the readings stored to a file for subsequent analysis. Figure 3 shows the silkscreen of the PCB, indicating the location of the thermocouples on the PCB.

Figures 4 through 6 summarize the results of the experiment. The positions indicated in the legend refer to the positions indicated in Fig. 3. In each of these figures, the SRG is generating for approximately 22 minutes at which time its output is reduced to zero. While generating, the dc bus current is 19 A, the phase currents are 15 A, the output power is 5.7 kW, the SRG efficiency is 87.3% and the inverter efficiency is 90.8%. The thermocouple readings are stabilized by running the coolant loop prior to exciting the SRG.

Figure 4 shows the temperature evolution in one corner of the PCB in comparison to the temperature

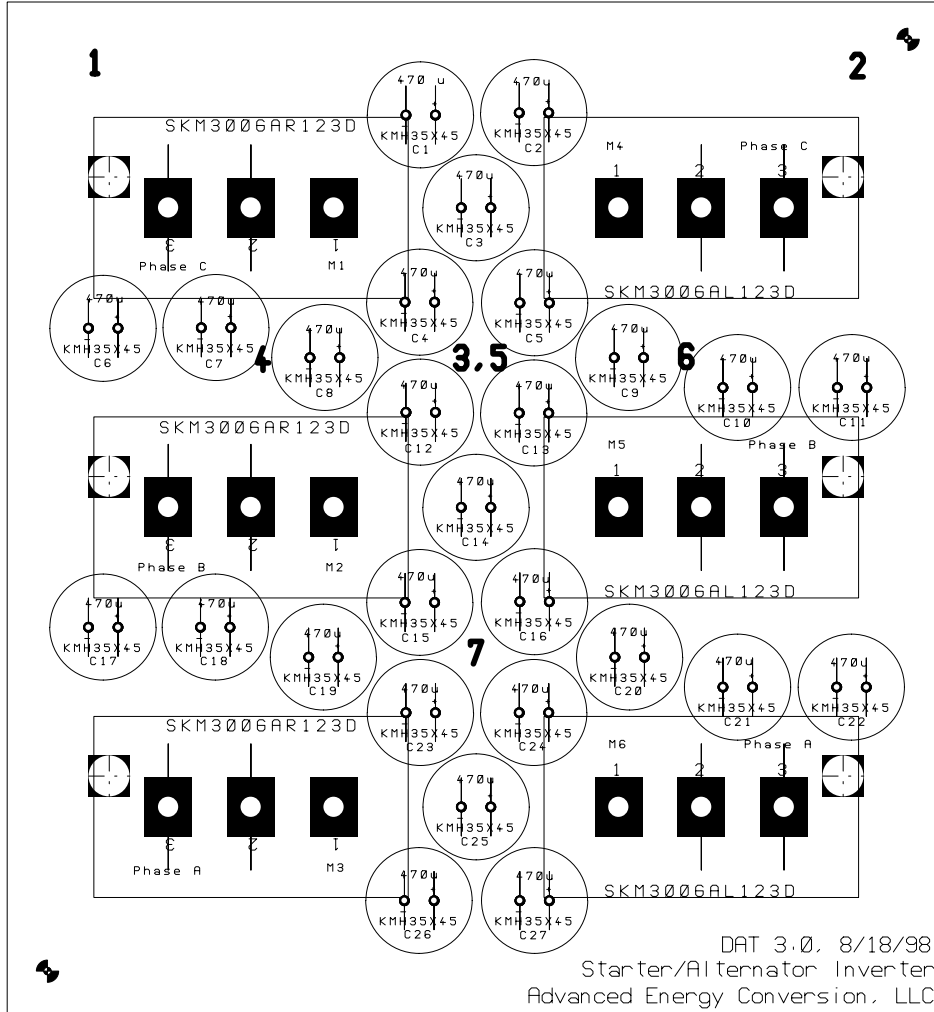


Figure 3: The silkscreen for the PCB modeled and evaluated experimentally. The circles are capacitors, the rectangles are IGBT modules, and the **bold** numbers correspond to thermocouple locations.

evolution at an interior location. The temperatures track quite closely, with a small temperature difference. This suggests that the temperature across the board is relatively uniform. While steady state temperatures are not reached, the projected temperature rise is consistent with the calculations of Sec. 3 to first order.

Figure 5 shows the temperature evolution on both sides of the PCB. The tight tracking of the temperatures suggests that the thermal resistance through the PCB structure is negligible. This is consistent with the model developed in Sec. 3.

Figure 6 shows the temperature evolution at three interior locations on the PCB. The more rapid initial rise of the temperature at the central location

followed by consistent tracking of the three temperatures suggests some initial heat diffusion from the central location to the outer locations. This diffusion can also be observed after the SRG output is brought to zero.

5 Application Issues

The application of PCBs to integrate the construction of power electronic converters has its limitations and important considerations, which include:

1. Only planar structures can be accommodated effectively. This can present problems for designs that require the use of device modules that

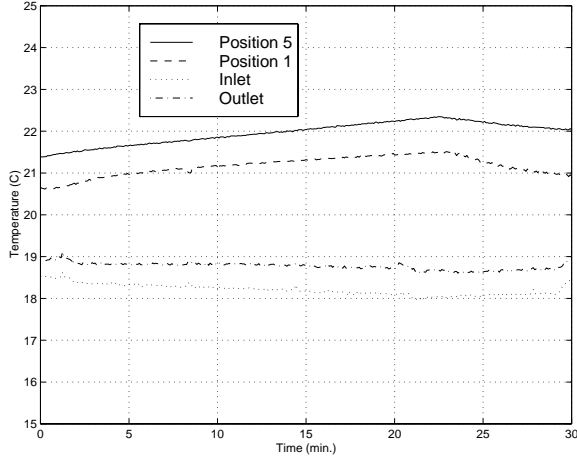


Figure 4: The temperature evolution near the edge of the PCB and at an interior point.

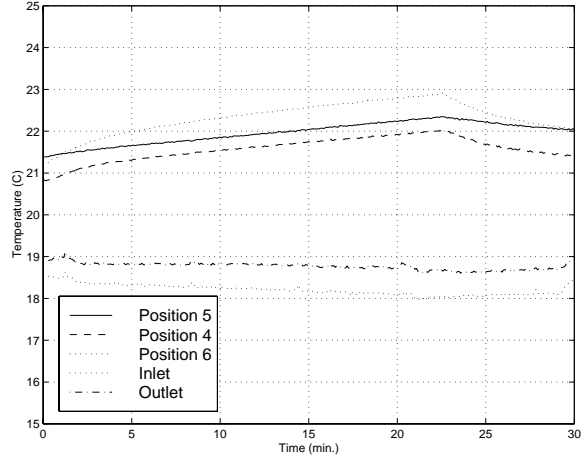


Figure 6: The temperature evolution at three interior points.

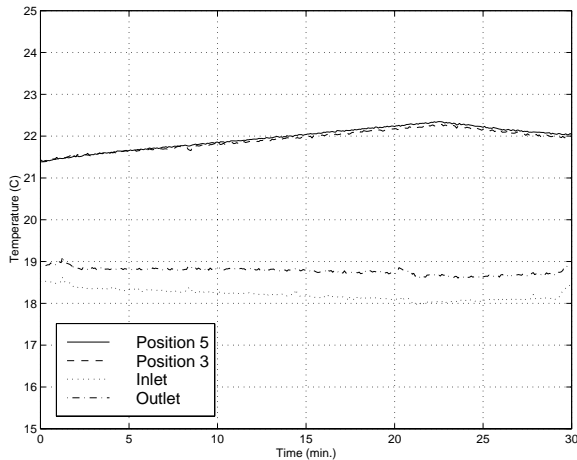


Figure 5: The temperature evolution on each side of the PCB at an interior point.

do not have the same height.

2. Copper cladding thickness cannot be made arbitrarily thick without special manufacturing costs. These costs will erode any benefit of the technique over laminated bus bars. However, converters can be accommodated with this technique up to very high power levels. A rule of thumb is to keep the current density to less than 500 A/cm^2 within the copper traces or zones.
3. Thermal cycling of the PCB should be minimized. Excessive thermal cycling creates internal stresses within the PCB that could lead to

delamination. As indicated in Table 2, the copper expands at nearly twice the rate as the FR-4 leading to shear stress on the bond between the copper and FR-4. Further, vias can be damaged due to thermal cycling [11].

4. Short circuit conditions need careful consideration to ensure survivability [11].

6 Summary

This paper has presented a discussion of the issues surrounding the application of printed circuit boards to power electronic converters. The concept is particularly useful in the prototyping of a power electronic converter where prototype laminated bus bars are expensive and have long lead times. The issues associated with using the PCB are largely thermal, with the heat being driven by the losses within the copper layers of the PCB as they support the relatively large currents within the power converter.

We have shown how to develop a simple analytic thermal model of a PCB to help guide the design process. The model developed here reflects the design of a PCB used to support the inverter for a SRG. This model is compared with the experimental performance of a PCB to show that the model is valid to first order.

Acknowledgements

The development of the prototype starter/alternator system described in this paper was supported by Dana Corporation. The assistance of Al Smith and Narongsak Thongpapanl with instrumentation and measurement is gratefully acknowledged

References

- [1] R. J. Whistler, "Laminated bus bars eliminate unmanageable cabling in high power systems cabinets," PCIM Power Electronics Systems, pp. 70-75, June 1999.
- [2] J. P. Holman, *Heat Transfer*, 4th ed., McGraw-Hill, 1976.
- [3] A. F. Mills, *Basic Heat and Mass Transfer*, Irwin, 1995.
- [4] National Electrical Manufacturers Association, "Industrial laminated thermosetting products," Standard LI 1-1998.
- [5] Institute for Interconnecting and Packaging Electronic Circuits, "Design standard for rigid printed boards and rigid printed board assemblies," ANSI/IPC-D-275, 1991.
- [6] W. T. Shugg, *Handbook of Electrical and Electronic Insulating Materials*, 2nd ed., IEEE Press, 1995, Chapter 9.
- [7] D. Christiansen, ed., *Electronics Engineer's Handbook*, McGraw-Hill, 1997, Chapter 9.
- [8] H. Johnson and M. Graham, *High Speed Digital Design: A Handbook of Black Magic*, Prentice Hall, 1993, pp. 217-221.
- [9] J. M. Kokernak, D. A. Torrey and M. Kaplan, "A switched reluctance starter/alternator for hybrid electric vehicles," *Power Electronics Proc. (PCIM Conference)*, pp. 74-80, 1999.
- [10] E. Mese, Y. Sozer, J. M. Kokernak and D. A. Torrey, "Optimal excitation of a high speed switched reluctance generator," *Proc. of the IEEE Applied Power Electronics Conf.*, pp. 362-368, 2000.
- [11] R. Tarzwell, "High power tests determine design requirements for P. C. board survivability," PCIM Power Electronic Systems, pp. 66-72, June 2000.